Materials Science in Semiconductor Processing 41 (2016) 420–427

Contents lists available at ScienceDirect

Materials Science in Semiconductor Processing

journal homepage: www.elsevier.com/locate/mssp

Quantum confinement and size effects in Cu_2ZnSnS_4 thin films produced using solution processed ultrafine nanoparticles

Amna Safdar [a], Mohammad Islam [b,*], Iftikhar Ahmad [b], Aftab Akram [a], Mohammad Mujahid [a], Yasir Khalid [b], Yanqiu Zhu [c]

[a] School of Chemical and Materials Engineering, National University of Sciences and Technology, Islamabad 44000, Pakistan
[b] Center of Excellence for Research in Engineering Materials (CEREM), Advanced Manufacturing Institute, King Saud University, P.O. Box 800, Riyadh 11421, Saudi Arabia
[c] College of Engineering, Mathematics and Physical Sciences, University of Exeter, Exeter EX4 4QF, UK

ARTICLE INFO

Article history:
Received 31 May 2015
Received in revised form
28 September 2015
Accepted 29 September 2015

Keywords:
Cu_2ZnSnS_4
CZTS Nanoparticles
Thin Films
Quantum Confinement
Size Effect

ABSTRACT

Copper–zinc–tin-sulfide (Cu_2ZnSnS_4, abbreviated as CZTS) is a direct band gap p-type semiconductor material with high absorption coefficient. Using oleylamine as solvent/stabilizing agent and metal chlorides and sulfur particles as chemical precursors, CZTS based nanoparticles were produced and subsequently deposited as thin films on glass substrates via spin coating of the nanoinks. The effect of temperature on crystallite size and phase composition was assessed after the solution mixture was undercooled by 30, 70 or 90 °C. Upon cooling the solution from 230 to 140 °C i.e. by 90 °C, maximum refinement in the nanoparticles size was noticed with average size on the order of few nanometers. The morphological and compositional studies of the nanoparticles were performed by means of scanning electron microscope, X-ray diffraction and Fourier transform infrared spectroscopy techniques. Phase-pure CZTS formation was confirmed from fast Fourier transform (FFT) patterns and lattice fringes observed during HR-TEM examination. Characterization of the annealed spin coated films, made from nanoink containing ultrafine nanoparticles, indicated morphological changes in the film surface during air annealing at 350°C that can be attributed to depression of CZTS phase decomposition temperature. Spectrophotometric studies of the annealed films suggested quantum confinement effect through an associated increase in the band gap value from 1.34 to 2.04 eV upon reduction in the nanoparticle size caused by increasing the degree of undercooling to 90 °C.

1. Introduction

Thin film solar cells based on chalcogenide materials, such as copper–indium–gallium-(di)selenide (CIGS) and cadmium telluride (CdTe), have been reported to exhibit record conversion efficiencies of 21.7 [1] and 20.4%, respectively [2]. Technologies based on these absorber layers has already entered commercialization phase with power conversion efficiencies of ~15% [3]. The issues of cost, rareness and toxicity, however, are to be dealt with and an alternative earth abundant, eco-friendly composition with similar performance attributes for scale-up is needed. A quaternary sulfide compound with typical chemical composition of Cu_2ZnSnS_4 (CZTS) is a self-doped, p-type semiconductor compound in which In and Ga of CIGS are replaced by Cu and Zn cations, respectively, via assignment of the same Wyckoff positions and tendancy to crystallize in the more stable kesterite crystal structure [4–6]. A high absorption coefficient value ($> 10^4$ cm^{-1}) corresponding to a direct band gap of 1.40–1.50 eV and use of earth-abundant natural resources makes CZTS based PV technology more cost-effective [7–8].

There are a number of vacuum based techniques that have been employed in thin film PV technology due to their high yield and cost-effectiveness [9]. The solution based methodologies utilizing wet chemistry need further studies in order to optimize the optoelectronic properties to produce high quality uniform films [10–13]. There are extra degrees of freedom associated with a quaternary compound that allows the possibility of adjusting the composition and, therefore, the materials properties, which is an advantage over binary materials for thin film light absorbers.

The chemical compounds such as oleylamine and trioctylphosphineoxide can act as solvents as well as capping agents for size-controlled synthesis of chalcogenide compositions [14–17]. After parametric studies on process optimization for other component films namely Mo back contact [18], ZnO produced using RF-plasma

* Corresponding author. Fax: +966 11 46 70 199.
E-mail addresses: mohammad.islam@gmail.com, miqureshi@ksu.edu.sa (M. Islam).

http://dx.doi.org/10.1016/j.mssp.2015.09.027
1369-8001/

magnetron sputtering [19] and sol–gel deposition [20] and CdS buffer layer [21,22], our research is focused on the development of solution based synthesis routes for different absorber layer compositions.

In this paper, we investigate the effect of degree of undercooling on the size and composition of resulting nanocrystals using metal precursor salts, sulfur powder and oleylamine. Nanoinks made from the nanocrystals were spin coated onto soda-lime glass and air annealed at 350 °C. The nanocrystal size refinement noticed upon increasing the degree of undercooling is manifested during optical band gap measurement and microstructural characterization of the annealed film. The facile, one-pot synthesis route developed during this research can be very useful towards synthesis of phase pure CZTS nanocrytals and thin films with controlled size and properties.

2. Methods

2.1. Synthesis of CZTS based Nanoparticles

All the chemical reagents used for this study were of analytical grade (> 99.9% purity; Sigma Aldrich) and were used without any treatment. Metal halides of copper, zinc and indium in the form of copper iodide (CuI), zinc chloride ($ZnCl_2$) and tin chloride ($SnCl_2$) were used as chemical precursors along with sulfur (S) powder. For synthesis of nanoparticles, 90, 40 and 60 mM of CuI, $ZnCl_2$ and $SnCl_2$ respectively, were dissolved in oleylamine (OAm) and heated to 170 °C for 30 min until a clear solution was obtained. Another solution of S powder (200 mM) in OAm was prepared. The molar ratio Cu:Zn:Sn:S of 90:40:60:180, when normalized, approximates to be 2.00:0.89:1.33:4.00. Both solutions were mixed together and the resulting mixture was heated to 230 °C for 90 min to ensure complete chemical reaction between precursor species. The solution was subsequently cooled and further purified by pouring into cold methanol. The effect of the degree of undercooling on the size and composition of nanocrystals was investigated by cooling the solution from 230 °C to 200, 160 or 140 °C. Subsequent washing of the nanocrystals was repeatedly carried out through centrifugation after which the black powder residues were dried in a vacuum oven at 40 °C for 18 h.

2.2. Thin film deposition

The nanoink of the powder from each processing condition was made by adding 200 mg of powder in chloroform. To ensure deflocculation and uniform dispersion, an ultrasonic treatment was carried out for a period of 20 min. Thin films from the ink so prepared were deposited on the 15×25 mm^2 soda-lime glass substrates via spin coating of the nanoinks under inert atmosphere for the same spin cycles followed by atmospheric annealing at 350 °C for 30 min. In this paper, the powder and thin film samples prepared after undercooling the solution by 30, 70 and 90 °C are denoted with a prefix *p* and *f*, respectively, as listed in Table 1.

2.3. Compositional, structural and functional characterization

The phase purity and crystallinity of the absorber CZTS films were characterized by X-ray Diffraction (XRD) machine (STOE Stadi MP) using a monochromatic CuKα radiation (1.5405 Å) at 30 kV operating voltage and emission current of 12 mA. The diffraction patterns were obtained for 2θ values in the range of 5–80° with step size and scan rate of 0.01° and 2 °/min, respectively. From XRD results, the crystallite size *t* for the phases present was computed using Scherrer relation

Table 1
Sample identification and processing conditions for CZTS nanoparticles and films.

S.N.	Sample ID	Precursor ratio (mM) CuI: $ZnCl_2$: $SnCl_2$: S 90: 40: 60: 180 or 2.00: 0.89: 1.33: 4.00	Process variable Degree of undercooling (°C)
1.	*p-30*	Dried powders	30
2.	*p-70*		70
3.	*p-90*		90
4.	*f-30*	Annealed films	30
5.	*f-70*		70
6.	*f-90*		90

$$t = 0.94\,\lambda \,/\, [\{(B_M)^2 - (B_S)^2\}^{1/2} \cos\theta]$$

where λ and θ are the wavelength of the Cu-Kα radiation and diffraction angle, respectively, the constant 0.94 refers to the shape factor value for spherical particles. The terms B_M and B_S represent full-width-at-half-maximum for the diffraction peak and the standard (SiO_2) with the value for the latter to be 0.080.

The presence of surface chemical bonds on the nanoparticles surface was investigated using attenuation-total-reflection, Fourier transform infrared spectroscopy (ATR-FTIR) (JASCO FTIR-4100) for the wavenumbers in the range of 400–4000 cm^{-1}.

The nanocrystals size and morphology was determined from microstructural examination using field-emission scanning electron microscope (FE-SEM) (JSM7600F) and field-emission transmission electron microscope (FE-TEM; JEOL JEM-2100F and JEOL 2000 FX, Japan) with accelerating voltage of 200 kV, LaB_6 electron gun and 0.18 nm point-to-point resolution. Surface topography of the spin coated films was done using scanning electron microscope (JEOL JSM7600F) operating at 5 kV. Energy dispersive spectrum (EDS) analysis of the films was performed using Oxford Instruments X-act detector. For each sample, the EDS analysis was performed on a large area and the composition was averaged using three sets of measurements.

The band gap energy (E_g) values of the CZTS thin films were determined using optical spectrophotometer (Labomed UV2500). The optical absorption spectra for all the samples were obtained at room temperature in the 200–1200 nm wavelength range. The nature of direct optical inter-band transition was estimated from Tauc plots using the equation, $\alpha = \alpha_o(h\nu - E_g)/h\nu$, where α is the absorption coefficient, $h\nu$ is the incident photon energy corresponding to the wavelength value and E_g is the band gap energy value.

3. Results and discussion

3.1. Phase and composition analysis

X-ray diffraction (XRD) studies were performed on the powders produced from undercooling of the solution mixture by 30, 70 and 90 °C as well as the spin coated films prepared using nanoinks. The dried CZTS based powders depict polycrystalline nature, as evident from the presence of several diffraction peaks, shown in Fig. 1(a). Several peaks at various diffraction angles are observed corresponding to different planes of tetragonal CZTS phase with kesterite structure, in accordance with the powder diffraction file (JCPDS 20-0575) of the International Center for Diffraction Data. The weak diffraction peak at ~30° indicates a small fraction of hexagonal phase CZTS formation beside the tetragonal phase. An additional weak peak at ~43° for the sample *p-30* signifies slightly

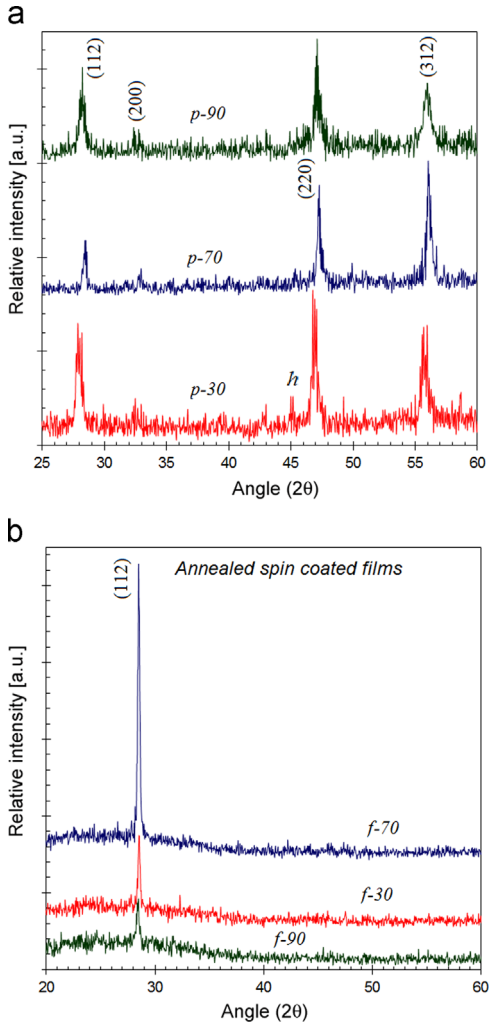

Fig. 1. X-ray diffraction patterns of the CZTS samples produced after different degrees of undercooling (Table 1): (a) dried powders and (b) thin films after a certain number of spin cycles.

large fraction of hexagonal phase nanocrystals. The relatively low intensity and high breadth of the diffraction peaks is mainly due to low crystalline quality of the nanoparticles in the absence of annealing step. Using nanoinks made from the dried powders, thin films were deposited over glass substrates via spin coating and subsequently annealed. Although the *f-30* and *f-70* films were prepared from 3 spin coating cycles, the sample *f-90* was produced after 7 spin cycles to observe any diffraction peaks. The XRD patterns, shown in Fig. 1b, indicate that films prepared from different samples represent predominantly one crystallographic orientation with good crystalline quality as manifested by the sharper (112) peak. Thus, the annealing treatment is found to enhance crystalline quality and promote a particular crystallographic orientation in the CZTS phase.

For dried powders, the crystallite size values, computed from the two main diffraction peaks using Scherrer equation (Table 1), indicate a slight increase upon increasing the degree of undercooling from 30 to 70 °C followed by a decrease. For annealed films, while the crystallite size is in the same range for *f-30* and *f-70* samples, the crystallite size for *f-90* is determined to be ~18 nm for the film produced after 7 spin cycles. As compared to dried powder (*p-90*), the reduction in crystallite size upon annealing (*f-90*) suggests some degree of CZTS phase decomposition although no additional peaks corresponding to any other phase appear in the XRD pattern.

Table 2
EDS analysis and crystallite size data computed using Scherrer equation.

ID	EDS Analysis (at%)				Cu/(Zn+Sn)	Zn/Sn	Cu/S	Crystallite size (nm)	
	Cu	Zn	Sn	S				(112)	(220)
p-30	21.7	9.4	20.4	48.5	0.73	0.46	0.45	51.4	33.8
p-70	23.6	10.1	16.2	50.1	0.90	0.62	0.47	46.0	44.8
p-90	21.2	10.5	17.9	50.4	0.75	0.59	0.42	26.8	35.0
f-30	24.9	13.0	16.6	45.5	0.84	0.78	0.55	33.9	–
f-70	25.2	14.1	18.0	42.7	0.79	0.79	0.59	48.6	–
f-90	24.2	13.1	13.9	48.8	0.90	0.94	0.49	18.4	–

In case of dried powders, the EDS analysis for *p-30* indicates presence of peaks characteristic of Cu, Zn, Sn and S beside weak peaks (due to substrate and contamination) from Si, C and O. The elemental composition (at%) and the values of Cu/(Zn+Sn) and Zn/Sn obtained from EDS analyses are given in Table 2. The analysis was performed at three different areas and then the values obtained were averaged. From the data, all the powders appear to exhibit Sn-rich and Zn-poor composition. The Cu/(Zn+Sn) values given in Table 2 suggest formation of Cu-poor composition for all the samples. The resulting composition is almost stoichiometric for the sample *p-70* in terms of Cu/(Zn+Sn) ratio, though Zn/Sn and Cu/S values for *p-70* and *p-90* are in close proximity to each other. Compared to the typical atomic ratio of 2:1:1:4 in the Cu_2ZnSnS_4 composition, the Zn content is found to be slightly deficient showing an increase from 9.4 to 10.5 (at%) upon increasing the degree of undercooling. A possible reason for low Zn incorporation into the CZTS film maybe a relatively higher reactivity of the chloride salts compared to the Zn ions [14], which in turn, improved for greater degree of undercooling.

Upon annealing, although the overall composition for all the samples remained Zn-poor, the samples became slightly richer in Zn, as indicated by higher Zn/Sn values, owing to Sn and S loss to some extent. Nevertheless, a Cu-poor starting precursors' ratio and Zn-poor annealed film composition suggest Cu_2SnS_3 phase formation during annealing through chemical reaction between Cu_2S and SnS_2 to an extent that is too small to be detected in XRD patterns. There was an associated decrease in the S content as manifested by a corresponding slightly higher Cu/S values in the range of 0.49–0.59, compared to its theoretical value of 0.5. The reduction in S content during annealing treatment is presumably due to its evaporation either as unreacted S or low melting temperature phases such as SnS_2 and Cu_2S [8]. When compared to dried powders, the annealing treatment is noticed to slightly lower the amount of S in the films. It is noteworthy, however, that the quantitative information derived from EDS analysis is not very reliable due to close proximity of Cu and Zn on the periodic table and the subsequent difficulty in differentiating characteristic X-rays from these elements.

The FTIR spectra of the powder samples *p-30* and *p-90*, shown in Fig. 2, represent absorption bands at different positions that are characteristic of certain chemical bonding attributes. The weak shoulder band at 965 cm^{-1} is due to Si–O stretching mode vibrations from the substrate. It is an established fact that OAm [$H_3C(CH_2)_7HC{=}CH(CH_2)_8NH_2$] plays a critical role in the nanoparticles synthesis through acting as a solvent, stabilizing agent and reductant. OAm dissolves the metal halides forming metal-oleylamine complexes upon heating to intermediate temperatures (170 °C in this case). In a separate solution, OAm dissolves sulfur and reduces it to S^{2-} ions since it is an electron donor at elevated temperatures. Upon mixing the two solutions, the metal ions react with S^{2-} ions to make CZTS based nanoparticles [23,24]. Subsequent attachment of OAm to the growing nanoparticle dictates

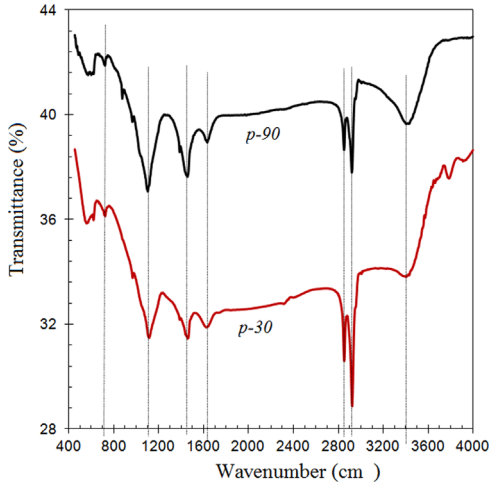

Fig. 2. FTIR spectra of the dried powders produced with an undercooling of 30 (*p-30*) and 90 °C (*p-90*).

the particle size through its role as a capping ligand. The degree of cooling has an important role towards growth of such nanoparticles, as noticed during HR-TEM examination (discussed later). The presence of sharp, strong bands at ~2875 and 2940 cm^{-1} are indexed to be due to OAm. The weak band at 619 cm^{-1} maybe due to C–C bending mode vibrations. The broad band at ~3430 cm^{-1} can be attributed to OH stretching vibrations of H_2O or asymmetric/symmetric NH stretching vibrations owing to the metal-thiourea complexes [25]. The role of oleylamine towards CZTS formation and as capping ligand is manifested through presence of bands with characteristic modes that represent oleyl groups located at 2851–2853 and 2922–2925 cm^{-1} beside presence of bending and symmetric/asymmetric stretching modes representing metal-thiourea complexes. Despite the same extent of band broadening, a decrease in intensity of the 1109 cm^{-1} peak implies higher levels of hydroxyl and S additions in the *p-30* powder sample, as supported by the presence of more intense peaks in the 2800–3000 cm^{-1} regime.

3.2. Morphological studies

The morphological examination of the powders was carried out using FE-SEM, as shown in Fig. 3. For the dried powder sample (*p-30*), the particles are noticed to be polydisperse with a broad size range. While the seemingly large particles maybe clusters of few hundred nanometers, fine nanoparticles of the sub-100 nm size are also evident. It is highly likely that, upon cooling from 230 to 200 °C, fewer nuclei formed resulting in their subsequent growth to large sizes. Nevertheless, very fine particles with < 10 nm size are also seen (Fig. 3c). Upon cooling the solution mixture from 230 °C to lower temperatures namely 160 and 140 °C, the nanoparticles produced were monodisperse with a progressive decrease in the average particle size.

The results from TEM examination of the dried nanoparticles are shown in Figs. 4–6. In case of the powder *p-30*, the

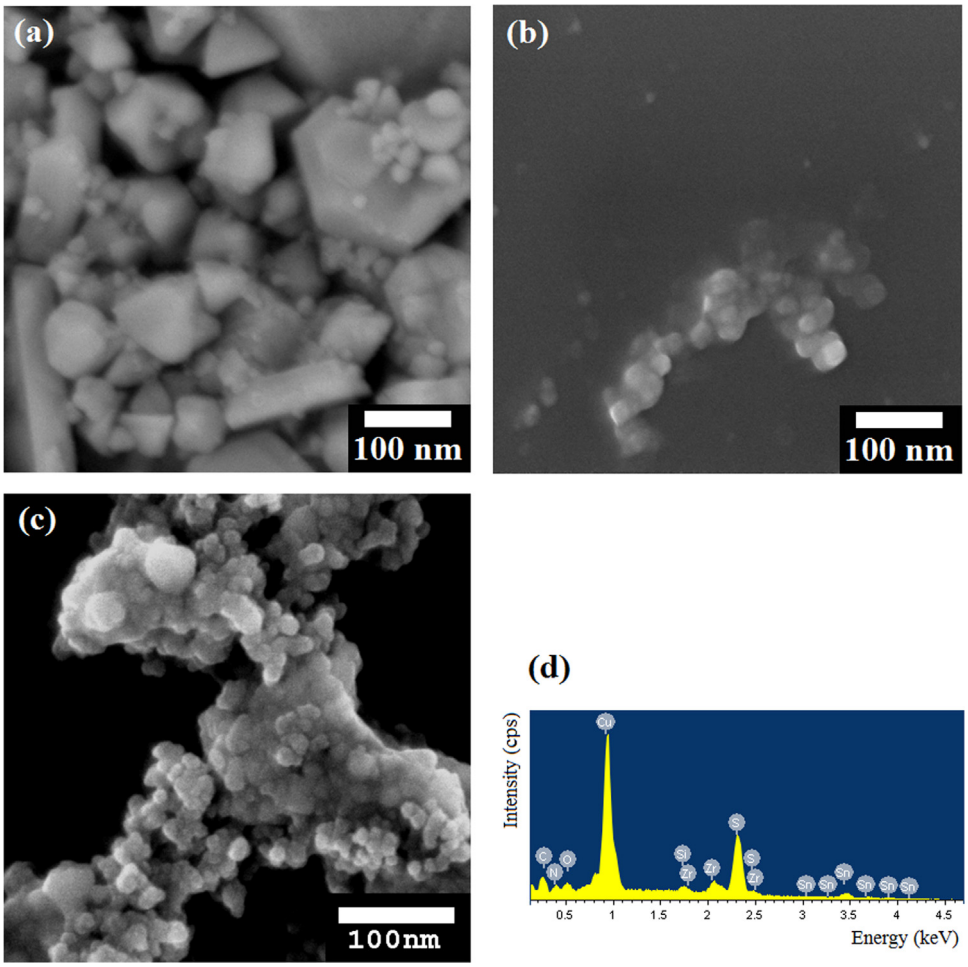

Fig. 3. FE-SEM microstructures of CZTS powders produced with an undercooling of: (a) 30 °C (*p-30*), (b) 70 °C (*p-70*) and (c) 90 °C (*p-90*); and (d) EDS results of the powder *p-30*.

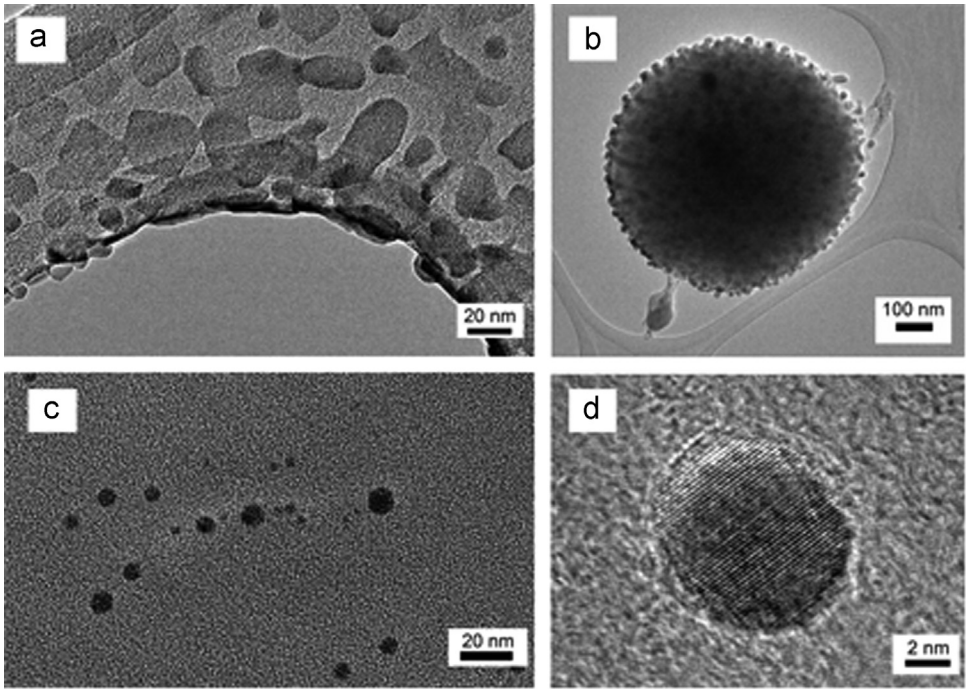

Fig. 4. Microstructural examination of the *p-30* CZTS powder: (a, b) Nanoparticles with different sizes and morphologies, (b) a large cluster made up of fine nanoparticles, (c) low magnification view of several individual spherical-shaped nanoparticles, and (d) HRTEM image of an individual nanoparticle.

polydisperse nature of particles and variation in shape is evident from low magnification microstructure shown in Fig. 4a. Although individual nanoparticles, spherical in shape with typical size of < 15 nm are clearly evident in Fig. 4c, their tendency to agglomerate is manifested by appearance of a large cluster made up of numerous fine particles (Fig. 4b). The cluster size is ~0.75 μm with presence of very fine individual nanoparticles at its periphery. The HRTEM microstructure of one such fine particle with an estimated size of ~8.7 nm is shown in Fig. 4d.

When the solution mixture was cooled from 230 to 160 °C as in case of the powder *p-70*, a further reduction in the nanoparticles size was observed. Fig. 5a shows a large cluster of ~50 nm formed due to agglomeration of several fine particles, while in Fig. 5c, individual nanoparticles (indicated by circles) mostly spherical in

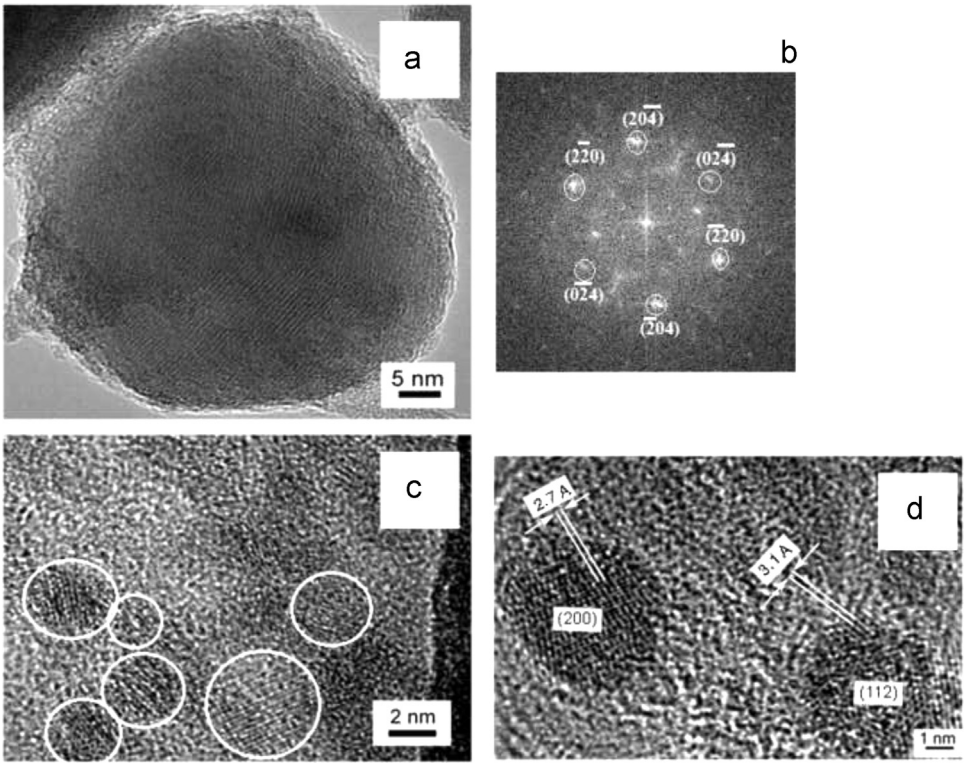

Fig. 5. Electron microscopy results of the *p-70* CZTS powder: (a) Clustering of several nanoparticles, (b) FFT pattern calculated from a, (c) HRTEM microstructure of ultrafine nanoparticles dispersed on amorphous carbon film of the lacey grid and (d) high magnification view of nanoparticles showing diffraction fringes.

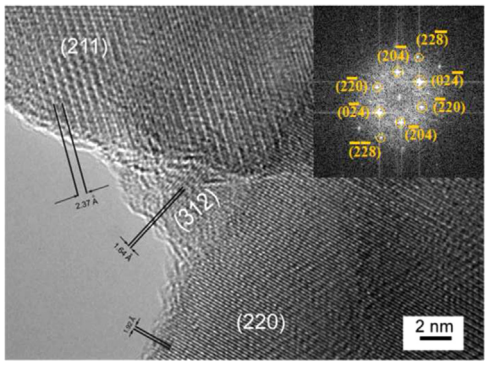

Fig. 6. (a) HRTEM image of CZTS *p-90* and (b) FFT pattern showing polycrystalline nature of the CZTS nanoparticles.

shape and having size of the order of ~5 nm can be clearly seen. Indexing of the lattice fringes indicates the nanoparticles to be belonging to the tetragonal CZTS phase (142 m group) with crystallographic planar indices of (112) and (200). The fast Fourier transform (FFT) pattern, obtained during HRTEM studies, is presented in Fig. 5c after indexing of different crystallographic planes. The formation of CZTS is confirmed from FFT pattern as well as inter-planar spacing values as determined from HRTEM examination. Although individual, isolated ultrafine nanoparticles could not be seen in case of the sample *p-90*, diffraction fringes observed (Fig. 6) as well the corresponding FFT pattern (inset) confirmed CZTS formation.

Since a reduction in the nanoparticle size leads to an increase in its surface area as well as higher defect density owing to broken bonds, the melting temperature (T_m) of the particles is less than that of the bulk material. In case of tin nanoparticles, a reduction in the T_m value from 232.6 (bulk) to 214.9 °C (26 nm) was reported [26]. Another study reported a temperature drop for the solid-solid phase transition from monoclinic low-chalcocite to hexagonal high-chalcocite Cu_2S structure from its value of ~104 °C for the bulk phase to 52 °C for the Cu_2S nanorods [27]. Similar effect is observed in semicrystalline polymer thin films where the thickness value below a certain threshold not only depresses the melting temperature below its value for the bulk material, it also hinders crystallization [28]. Both factors namely the nanoparticle size and the film thickness are speculated to be instrumental in our case, causing melting point depression in the CZTS films and the subsequent change in the film morphology after annealing of the *f-90* films. The thickness values for all the annealed films are expected to be of the order of ~1 μm. For the films prepared with *p-90*, however, the effect of film thickness on melting behavior needs to be further investigated.

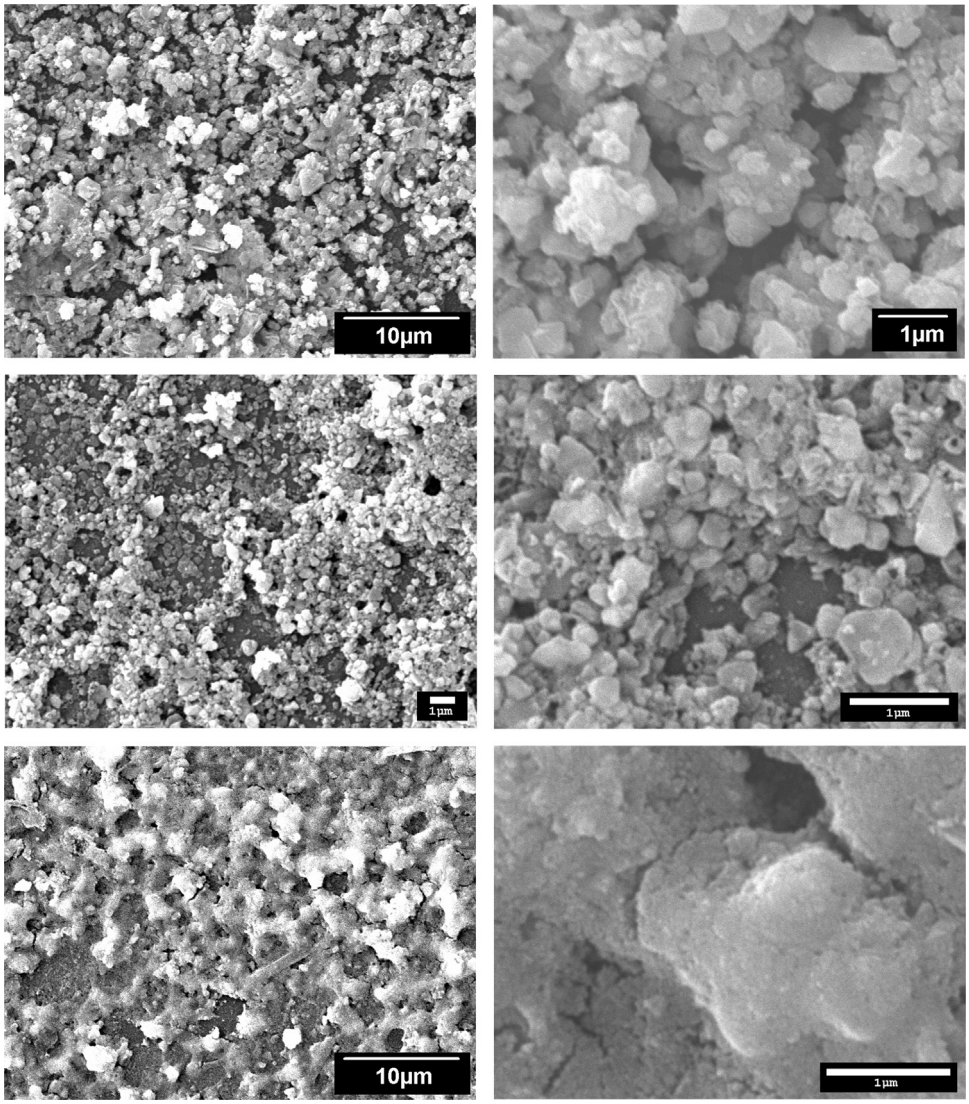

Fig. 7. Low and high magnification SEM microstructures of the CZTS film surfaces after annealing at 350 °C in air: (a, b) *f-30*, (c, d) *f-70* and (e, f) *f-90*.

Low and high magnification images of the different CZTS thin films, after annealing at 350 °C in air, are shown in Fig. 7. The film thickness values are anticipated to be in the same range since the composition of the nanoinks and the deposition conditions are identical in all cases. From comparison of the high magnification microstructures, it is evident that as the degree of undercooling is increased from 30 to 70 °C during powder synthesis, the nanoparticle size forming the micron-size clusters in the annealed films becomes more refined owing to the larger driving force towards nucleation of CZTS crystallites. This finding is also confirmed from HR-TEM examination of the powders. For *f-90* sample, a strikingly different surface morphology is revealed (Fig. 7e and f). Instead of the clusters consisting of the nanoscale crystallites, the surface appears continuous with presence of few cracks.

The decomposition temperature of the CZTS phase is 550 °C [29]. The change in surface morphology upon annealing at 350 °C in case of the *f-90* film may be attributed to one of more the following factors: (i) a depression in the CZTS decomposition temperature value due to size effect and (ii) formation and sublimation of a low T_m phase that is S rich. In the former case, formation of ultra-fine nanoparticles is confirmed from HR-TEM studies where a decreasing size trend is observed with an increase in the degree of undercooling. Formation of any additional phase beside CZTS, if any, maybe possible in small fraction since the XRD patterns do not show peaks other than those characteristic of the CZTS phase. Further evidence in support of this argument comes from band gap energy (E_g) calculations (discussed in the next section) where an increase in the E_g value is seen.

3.3. Optical properties

From spectrophotometer studies, the absorption spectra were obtained and square of the product of absorption coefficient (α) and the photon energy ($h\upsilon$) i.e. $(\alpha h\upsilon)^2$ was plotted against energy ($h\upsilon$), as shown in Fig. 8. Through extrapolation of the curves, the band gap values for different annealed films were determined. The optimum E_g value for a single band gap device is reported to be in the range of 1.45–1.6 eV [30]. As the degree of solution undercooling is increased from 30 to 90 °C, the band gap value is noticed to exhibit an associated increase from 1.27 to 2.04 eV. It is interesting to note that the difference in E_g values for samples *f-30* and *f-70* is not very large, implying that both films consist of predominantly tetragonal CZTS phase (E_g~1.5 eV) with presumably some contribution from Cu_2SnS_3 (E_g~0.93 eV) [31]. Although

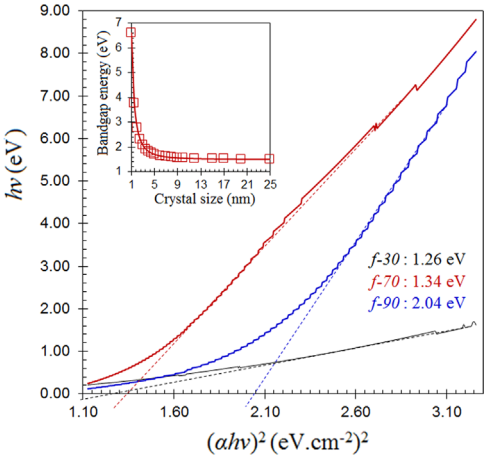

Fig. 8. (a) Graphical representation of $(\alpha h\upsilon)^2$–$h\upsilon$ data for the measured UV–vis absorption plots of CZTS films and the extrapolated linear fit to estimate the band gap energy at the *X*-axis intercept in each case. The inset shows theoretical prediction of E_g as a function of crystal size.

formation of the latter phase is not confirmed from XRD analysis, superposition of the strongest peak for CZTS and Cu_2SnS_3 as well as zinc-poor composition as determined from EDS analysis somewhat validate this assumption. The drastic increase in the E_g value to 2.04 eV as observed in case of *f-90* sample is considered to be due to very fine size of CZTS nanocrystals that exhibit quantum confinement effect. The finding is in agreement with earlier reports on quantum confinement effect in ultrafine nanoparticles [32,33]. The step-like behavior of the E_g, observed in case of *f-70* sample, has been attributed to the large defects concentration in the Sn-poor samples [34]. For spherical particles, the E_g value has inverse square dependence on the crystal size (t) as represented by equation $E(t)=E(\infty)+E_b(\pi a_B/t)^2$ where $E(\infty)$, E_b and a_B are bandgap energy for bulk CZTS, exciton binding energy and exciton Bohr radius with respective values of 1.5 eV, 28 meV and 4.3 nm [35]. The inset in Fig. 8 shows that there is significant increase in the E_g value once the crystal size is reduced below 7 nm. From comparison of theoretical and experimental E_g values, it is evident that although the crystallite size of 18.4 nm as calculated using Scherrer equation is slightly higher, TEM observations confirm that a significant fraction of the CZTS crystals in the *p-90* sample is less than 5 nm, thereby causing a drastic increase in the E_g value. On the other hand, although superfine nanocrystals with ≤ 10 nm size were seen during HRTEM studies of *p-30* and *p-70*, they virtually did not make any contribution towards any increase in the bandgap energy.

3.4. Nanocrystals and the annealing effect

For Cu-poor precursor ratio explored in this study with respective values of Cu/(Zn+Sn), Cu/Sn and Zn/Sn to be 0.90, 1.50 and 0.67, a possible explanation of the annealing effect is outlined in this section. Upon initial heating stage during annealing, excess S present in elemental form may sublime or even melt when the temperature exceeds it melting point of 388.2 K causing formation of SnS_2, a low temperature phase that melts at 450 K. Both experimental studies as well as kinetic modeling of SnS_2 evaporation suggest a two-step reaction with formation of SnS solid phase and sulfur vapors (S_2) followed by SnS evaporation [36]. Further increase to 570 K leads to Cu_2S phase formation which upon reaction with molten SnS_2 results in Cu_2SnS_3 phase. The reaction between Cu_2SnS_3 and ZnS eventually promotes formation of phase-pure Cu_2ZnSnS_4 composition. The surface morphology of the *f-90* film might have evolved from flow of molten SnS_2 phase which in part may have evaporated as well as participated in a chemical reaction with Cu_2S during heating. The reaction schemes for both Cu-poor and Cu-rich precursor compositions, determined through in-situ X-ray diffraction studies, are described in reference [8]. The loss of Sn from the film top at elevated temperatures has been reported [30]. A recent study on computation of enthalpy of CZTS formation predicted exothermic nature of reaction between binary phases namely Cu_2S, ZnS and SnS_2 to form Cu_2ZnSnS_4 and hypothesizes that although these binary phases maybe present at high temperatures, provided the cooling rate is very low, the binary phases will react to form single multinary CZTS phase [37].

4. Conclusion

Ultrafine nanoparticles of the phase-pure CZTS composition were obtained using solution/particle hybrid approach involving precursor metal salts and sulfur powder in oleylamine and cooling the solution mixture at 230 °C by 30, 70 or 90 °C. Characterization of the dried powders indicated polycrystalline nature of the nanoparticles with predominantly tetragonal CZTS phase. HR-TEM studies suggested maximum degree of reduction in the

nanoparticle size in case of solution cooling from 230 °C to 140 °C, which can be attributed to less extent of Oswald ripening of the nucleated crystals. Annealing of the spin coated films at 350 °C in air promoted formation of CZTS structure with (112) preferred crystallographic orientation. There was an associated partial decomposition of the film due to high specific surface area of the ultrafine nanoparticles. Determination of the band gap energy (E_g) values pointed towards quantum confinement effect through an increase from 1.26 to 2.04 eV owing to the increase in the degree of undercooling from 30 to 90 °C. The melting behavior during annealing of the spin coated film is explained on the basis of comparison of experimental data with published thermodynamic and kinetic studies on the CZTS nanocrystals and thin films.

Acknowledgments

The authors gratefully appreciate research Grant for this work through the National Research Program for Universities by Higher Education Commission (HEC), Pakistan (NRPU no. 20-1603). The authors gratefully acknowledge the technical and financial support of the Research Center of College of Engineering, Deanship of Scientific Research, King Saud University, Saudi Arabia.

References

[1] P. Jackson, D. Hariskos, R. Wuerz, O. Kiowski, A. Bauer, T.M. Friedlmeier, M. Powalla, Phys. Status Solidi (RRL) 9 (1) (2015) 28–31.
[2] M.A. Green, K. Emery, Y. Hishikawa, W. Warta, E.D. Dunlop, Prog. Photovolt.: Res. Appl. 22 (2014) 701–710.
[3] D.B. Mitzi, T.K. Todorov, O. Gunawan, M. Yuan, Q. Cao, W. Liu, K.B. Reuter, M. Kuwahara, K. Misumi, A.J. Kellock, S.J. Chey, T.G. d Monsabert, A. Prabhakar, V. Deline, K.E. Fogel, IEEE 978 (2010) 640–645.
[4] S. Schorr, G. Gonzalez-Aviles, Phys. Status Solidi A 206 (2009) 1054–1058.
[5] H. Wang, Int. J. Photoenergy 2011 (2011) 10, http://dx.doi.org/10.1155/2011/801292.
[6] S. Siebentritt, A.S. Schorr, Prog. Photovolt.: Res. Appl. 20 (5) (2012) 512–519.
[7] M. Jiang, X. Yan, Cu2ZnSnS4 thin film solar cells: present status and future prospects, in: Arturo Morales-Acevedo (Ed.), Solar Cells-Research and Application Perspectives, InTech, Osaka, 2013.
[8] R. Schurr, A. Hölzing, S. Jost, R. Hock, T. Voβ, J. Schulze, A. Kirbs, A. Ennaoui, M. Lux- Steiner, A. Weber, I. Kötschau, H.W. Schock, Thin Solid Films 517 (2009) 2465–2468.
[9] M. Kaelin, D. Rudmann, A.N.T. Tiwari, Solar Energy 77 (2004) 749–756.
[10] Q. Guo, G.M. Ford, W.-C. Yang, B.C. Walker, E.A. Stach, H.W. Hillhouse, R. Agrawal, Amer. Chem. Soc. 132 (2010) 17384–17386.
[11] Q. Guo, H.W. Hillhouse, R. Agrawal, Amer. Chem. Soc 131 (2009) 11672–11673.
[12] T.K. Todorov, K.B. Reuter, D.B. Mitzi, Adv. Mater. 22 (2010) E156–E159.
[13] D.B. Mitzi, M. Yuan, W. Liu, A.J. Kellock, S.J. Chey, L. Gignac, A.G. Schrott, Thin Solid Films 517 (2009) 2158–2162.
[14] M.B.A. Pein, W.H.T. Rath, E. Maier, H. Amenitsch, F. Hofer, C.O. Kappe, G. Trimmel, Inorg. Chem. 50 (2011) 193–200.
[15] M. Kruszynska, H. Borchert, J. Parisi, J.K.- Olesiak, J. Amer. Chem. Soc. 132 (2010) 15976–15986.
[16] T. Kameyama, T. Osaki, K. Okazaki, T. Shibayama, A. Kudo, S. Kuwabata, T. Torimoto, J. Mater. Chem. 20 (2010) 5319–5324.
[17] X. Lu, Z. Zhuang, Q. Peng, Y. Li, Chem. Commun. 47 (2011) 3141–3143.
[18] M. Khan, M. Islam, A. Akram, Z. Qi, L. Li, Mater. Sci. Semicon. Proc. 27 (2014) 343–351.
[19] A. Achour, M.A. Soussou, K.A. Aissa, M. Islam, N. Barreau, E. Faulques, L. Le Brizoual, M.A. Djouadi, M. Boujtita, Thin Solid Films 571 (2014) 168–174.
[20] S. Salam, M. Islam, A. Akram, Thin Solid Films 529 (2013) 242–247.
[21] M. Alam, M. Islam, S. Salam, M. Mujahid, Surf. Rev. Lett. 21 (4) (2014) 1450059 (10pp.).
[22] S. Salam, M. Islam, M. Alam, A. Akram, M. Ikram, A. Mahmood, M. Khan, M. Mujahid, Adv. Nat. Sci.: Nanosci. Nanotechnol. 2 (2011) 045001 (6pp.).
[23] T. Rath, W. Haas, A. Pein, R. Saf, E. Maier, B. Kunert, F. Hofer, R. Resel, G. Trimmel, Solar Energy Mater. Solar Cells 101 (2012) 87–94.
[24] J. Tang, S. Hinds, S.O. Kelley, E.H. Sargent, Chem. Mater. 20 (22) (2008) 6906–6910.
[25] O. Zaberca, F. Oftinger, J.Y. Chane-Ching, L. Datas, A. Lafond, P. Puech, A. Balocchi, D. Lagarde, X. Marie, Nanotechnology 23 (2012) 185402 (11pp.).
[26] H. Jiang, K.-sik Moon, H. Dong, F. Hua, C.P. Wong, Chem. Phys. Lett. 429 (2006) 492–495.
[27] J.B. Rivest, l-K. Fong, P.K. Jain, M.F. Toney, A.P. Alivisatos, J. Phys. Chem. Lett. 2 (19) (2011) 2402–2406.
[28] J.H. Kim, J. Jang, W.-C. Zin, Macromol. Rapid Commun. 22 (6) (2001) 386–389.
[29] A. Weber, R. Mainz, H.W. Schock, J. Appl. Phys. 107 (2010) 013516 (6pp.).
[30] K. Jimbo, R. Kimura, T. Kamimura, S. Yamada, W.S. Maw, H. Araki, K. Oishi, H. Katagiri, Thin Solid Films 515 (2007) 5997–5999.
[31] S.C. Riha, B.A. Parkinson, A.L. Prieto, J. Am. Chem. Soc. 131 (2009) 12054–12055.
[32] A. Khare, A.W. Wills, L.M. Ammerman, D.J. Norrisz, E.S. Aydil, Chem. Commun. 47 (2011) 11721–11723.
[33] C. Malerba, C.L.A. Ricardo, M. Valentini, F. Biccari, M. Muller, L. Rebuffi, E. Esposito, P. Mangiapane, P. Scardi, A. Mittiga, J. Renew. Sustain. Energy 6 (2014) 011404 (12pp.).
[34] J.J. Scragg, T. Ericson, T. Kubart, M. Edoff, C.P.- Bjorkman, Chem. Mater. 23 (2011) 4625–4633.
[35] F.-J. Fan, L. Wu, M. Gong, G. Liu, Y.-X. Wang, S.-H. Yu, S. Chen, L.-W. Wang, X.-G. Gong, ACS Nano 7 (2) (2013) 1454–1463.
[36] U. Manzoor, M. Islam, L. Tabassam, S.-U. Rahman, Physica E 41 (2009) 1669–1672.
[37] S.V. Baryshev, E. Thimsen, arXiv:1403:4922 [cond-mat.mtrl-sci], 2014.